Carbon materials from high ash biochar for supercapacitor and improvement of capacitance with HNO_3 surface oxidation

Hong Jin, Xiaomin Wang, Zhengrong Gu*, Joseph Polin

Agricultural and Biosystems Engineering Department, South Dakota State University, PO Box 2120, 1400 North Campus Drive, AgE Building, SAE 221, Brookings, SD 57007, USA

HIGHLIGHTS

► Nanostructured carbon with high capacitance >200 F g^{-1} from biochar.
► Nanostructured carbon containing graphene nanosheets.
► HNO_3 hydrothermal oxidation greatly increase surface oxygen groups.
► HNO_3 hydrothermal oxidation greatly improved internal resistance.
► HNO_3 hydrothermal oxidation greatly improved the capacitance at higher current density.

ARTICLE INFO

ABSTRACT

The hierarchical carbon, with high specific surface area (2959 $m^2 g^{-1}$) and high pore volume (1.65 $cm^3 g^{-1}$) was prepared from sustainable feedstock – biochar, which was a waste from a thermochemical process optimized for bio-oil production, using KOH catalytic activation. The hierarchical carbon after HNO_3 treatment, as electrode materials, showed improved specific capacitance 260 F g^{-1} in 6 mol L^{-1} KOH at a current density of 0.6 A g^{-1}, while the specific capacitance of carbon without oxidation exhibits relative high (200 F g^{-1}) at a higher current density (0.5 A g^{-1}) after 2000 cycles. More importantly, the capacitive performances of the hierarchical carbons are much better than general bio-inspired activated carbons, ordered mesoporous carbons and commercial graphene, thus highlighting the success of preparing high performance supercapacitor electrode material from biochar and potential for improving economic viability of thermochemical biofuel processes by converting biochar to a high value added carbon materials.

Published by Elsevier B.V.

1. Introduction

Supercapacitor is an important electrical energy storage device for promoting widespread application of electrical automobiles, brake energy recovery systems as well as enhancing energy efficient of instruments requiring peak power source, include elevator, crane and locomotives. Pursuing advances in supercapacitors technology is also critical to satisfy needs for developing the future energy storage systems to promote using sustainable wind or solar electricity in rural areas as well as improve application of electrical automobiles. Ultimately, to achieve highly stable reversible electrical energy storage capacity and high power density in supercapacitors, carbon materials to fabricate electrodes, should possess a hierarchical mesoporous structure with high surface, high conductivity, suitable pore size distribution and long-term cyclability. Until now, the most hopeful research for increasing energy and power density of supercapacitors focused on innovative carbon materials [1]. Although advanced carbon materials, such as graphene [2], carbon nanotubes [3] and carbon onions from metal carbide [4] have shown high capacitance and high power density in electrochemical supercapacitors and hybrid supercapacitors, those advanced carbon materials will be significantly limited by high cost. In addition, most conventional synthesis methods for these innovative carbon materials involve application of toxic strong oxidants, such as chlorine, $KMnO_4$ and hydrazine. Therefore, hierarchical carbon materials, prepared form sustainable precursors with scalable processes, would be of great benefit to large scale application of supercapacitor in energy storage and conservation. As a result, high surface (>2000 $m^2 g^{-1}$) bio-inspired activated carbons, which can be used in electrical energy storage, have been prepared from multiple biomass precursors such as sunflower seed shell [5], rice hull [6], corn grains [7,8] and cypress [9]. Besides benefits of better

* Corresponding author. Tel.: +1 605 688 5372.
E-mail address: Zhengrong.gu@sdstate.edu (Z. Gu).

sustainability and lower cost, hierarchical porous carbon materials based on biomass provide the pathways for easy accessibility of electrolytes and fast transportation of ions because the macroporous channels of the raw material was retained after pyrolysis, while activation formed micropores within the channel walls.

The first stage in most processes for producing carbon materials from biomass is carbonization or pyrolysis, which could also be designed to produce biofuel simultaneously. It is well known that all thermochemical bioenergy conversion processes, include gasification, hydrothermal pyrolysis, fast pyrolysis and slow pyrolysis, generate a solid co-product or waste called biochar. This biochar, generated from biofuel platforms, has a significantly higher ash content than charcoal obtained through traditional carbonization processes. Until now, biochar generated in thermochemical conversion has only been used as a soil amendment or low grade fuel and viewed as non-suitable feedstock for high quality carbon materials [10], while only woody based biochar containing less than 20% ash, has been successfully converted to activated carbon with surface area >1000 m^2 g^{-1} through KOH chemical activation [11]. Furthermore high ash biochar were only upgraded to low quality carbon materials with low surface area (around 600 m^2 g^{-1}) [12]. Although graphene nanosheets have only been synthesized from bio-precursors with CVD method [13], carbon microstructure similar to graphene or oxidized graphitic nanosheets have been formed by pyrolyzing sucrose or caramel using mesopore silicate as a template [14] or cross-linked collagen gel in a nitrogen atmosphere [15]. Therefore, activation of high ash charcoal from protein rich precursors might be able to generate carbon materials with microstructure similar to activated graphene. On the other hand, distillers dried grains with solubles (DDGS), as major co-product of corn ethanol, is a low cost protein rich feedstock, which has been used as potential energy sources for producing bio-oil with about 67% heating value (higher heating value) of gasoline through thermochemical processes [16], and biochar (10–20% of DDGS) containing around 50% ash and minerals.

Besides specific surface area, pore size distribution, porous structure and electrical conductivity, surface functional groups also significantly affect the electrochemical performance of carbon materials. In general, surface functional groups, especially oxygen acidic groups (i.e. carboxy, phenol) increase specific capacitance of carbon materials by forming reversible redox pseudo-faradaic capacitor through reacting with KOH electrolytes and increasing wettability of porous surface [17,18]. Thus, surface oxygen-containing functional groups have been deliberately introduced by oxidation in HNO_3 [17].

In the present work, biochar from DDGS, a co-product, which was produced by thermochemically processing designed for maximum bioenergy production, was collected and chemically activated using KOH. After activation, hierarchical carbon was further treated with 4 mol L^{-1} HNO_3. These hierarchical carbon samples were characterized using different analytic approaches such as N_2 isothermal adsorption and TEM. The suitability, of the carbon obtained for electrodes in a supercapacitor, was evaluated by using a series of electrochemical techniques include cyclic voltammetry (CV), galvanostatic charge–discharge and electrochemical impedance spectrum (EIS).

2. Materials and experiments

2.1. Preparation of hierarchical carbon

Biochar generated from the pyrolysis of DDGS was activated with KOH (KOH/biochar = 0.075 mol g^{-1}) in an N_2 inert atmosphere at 950 °C. The DDGS pyrolysis process was optimized for bio-oil production, not biochar production. Biochar samples were mixed with solution of KOH and dried in conventional oven at 105 °C 48 h. These dried mixture were further dried at 400 °C in muffle furnace (chamber is 15 × 15 × 22 cm) in N_2 atmosphere (N_2 flow is 500 ml min^{-1}) for 6 h to remove structural water. Then activation was carried out at 950 °C, with heating rate 5 °C min^{-1}, for 3 h. After specified activation, activated samples were cooled within muffle furnace in same N_2 atmosphere. After cooling to room temperature (around 9 h), activated carbon samples were washed with 0.1 mol L^{-1} HCl at 100 °C with condensing, then washed with deionized water to pH 7 and dried at 105 °C overnight under vacuum.

Partial carbon samples were further modified with 4 M HNO_3 at 150 °C. In brief, 1 g of carbon was soaked into 20 mL 4 mol L^{-1} HNO_3 in a sealed PTFE reactor (50 ml) at 150 °C for 48 h, cooled and then filtrated, washed with water, until the PH of the filter liquor equaled 7. The filter cake was collected and dried in the oven with the temperature of 110 °C for overnight.

2.2. Analytical methods for biochar and hierarchical carbon samples

Isotherm adsorption of N_2 at 77 K was carried out using one ASAP 2010 Micropore analyzer. The specific surface areas were calculated using the Brunauer–Emmett–Teller (BET) equation. The total pore volumes were obtained at relative pressure 0.995 P_0, while micropore and mesopore volume and the pore size distribution were determined by the original DFT analysis model for carbon (Micromeritics Inc.) based on the N_2 isotherm adsorption data. Ash content of carbon materials was measured according to ASTM D 2866-94 (1999). The structure of activated carbon was also characterized with Raman Spectrum (Horiba LABRam confocal Raman microscope) at room temperature, using an excitation wavelength at 532 nm from a diode pumped solid-state laser, as well as TEM (Hitachi H-7000 FA) and SEM (HITACHI S-3400N). The water contact angle of prepared electrodes was analyzed with the static sessile drop method using VCA 2000 Contact Angle Video analyzer and applied to measure the hydrophilicity of each electrode. Surface oxygen content of activated carbon samples were analyzed with energy-dispersive X-ray spectroscopy (EDS) in SEM system, while oxygen contents of whole samples were obtained through analysis using an Elemental (CHNOS) Analyzer.

2.3. Supercapacitor fabrication and electrochemical characterization

For any of the electrochemical characterizations, the surface area of electrode is 1 cm^2. Meanwhile, the electrolytic medium is 6 mol L^{-1} KOH. The electrodes were prepared by pressing the slurry of hierarchical carbon, carbon black (conducting material from Fisher scientific) and PTFE (binder) with a mass ration of 8:1:1 on nickel foam. Two-electrode sandwich-type cells were built using a stainless coin cell (2032) with a microporous PP separator celgard-2400 between the electrodes. Two-electrode supercapacitors were assembled in the argon protected glove box.

Cyclic voltammetry (scan rate from 2 to 200 mV s^{-1}) and galvanostatic charge/discharge cycling (current density load from 100 to 1000 mA g^{-1}) were performed using a SP-150 multichannel potentiostat–galvanostat-EIS (Biologic, France). The electrical conductivity of the carbon materials was also measured through the impedance spectroscopy (i.e. frequency response analysis yields over the frequency ranging from 0.1 Hz to 100,000 Hz with potential amplitude of 5 mV) with a SP-150 multichannel potentiostat–galvanostat-EIS (Biologic, France). The values of specific capacitance was calculated from the galvanostatic discharge characteristics at current density of 100–1000 mA g^{-1}, and expressed in Farad per gram of electrode active material.

The specific capacitance of the electrode is calculated using Equation (1)

$$C = \frac{2I\Delta t}{m\Delta v} \tag{1}$$

In here, I is the charge or discharge current density, Δt is the corresponding charge or discharge time, m is one of the symmetry electrodes mass and ΔV is the total corresponding potential change.

3. Results and discussion

3.1. Physicochemical characterization of hierarchical carbon samples

Ash content of DDGS biochar used in this project was higher than 45%wt, with bulk density around 0.42 g cm^{-3}, while its BET surface area was less than 10 m^2 g^{-1}. DFT model simulation results according to the nitrogen adsorption−desorption curve (Fig. 1A),

indicated that there is well-developed mesoporous structure in the hierarchical carbon (Fig. 1B). As seen, the hierarchical carbon contains micro- and mesopores with a distribution of sizes between 1 and 10 nm and concentrates from 2 to 3 nm (calculated using a DFT model). Surface area, microporous and mesoporous volume of the hierarchical carbon were 2959 m^2 g^{-1} (calculated in the linear relative pressure range from 0.0 to 0.15 P_0), 0.83 and 0.42 cm^3 g^{-1} respectively (Table 1). In addition, according to methylene blue (MB) adsorption experiments, the hierarchical carbon adsorbed 750 mg g^{-1} MB in 20 min, which indicated fast mass transfer and inter-connected porous structure. Therefore, the pore structure of the hierarchical carbon is quite unique, as well as far different from traditional activated carbon and carbon molecular sieve, prepared from woody biomass or fossil feedstock, which generally show MB lower than 300 mg g^{-1}. The hierarchical carbon contained both
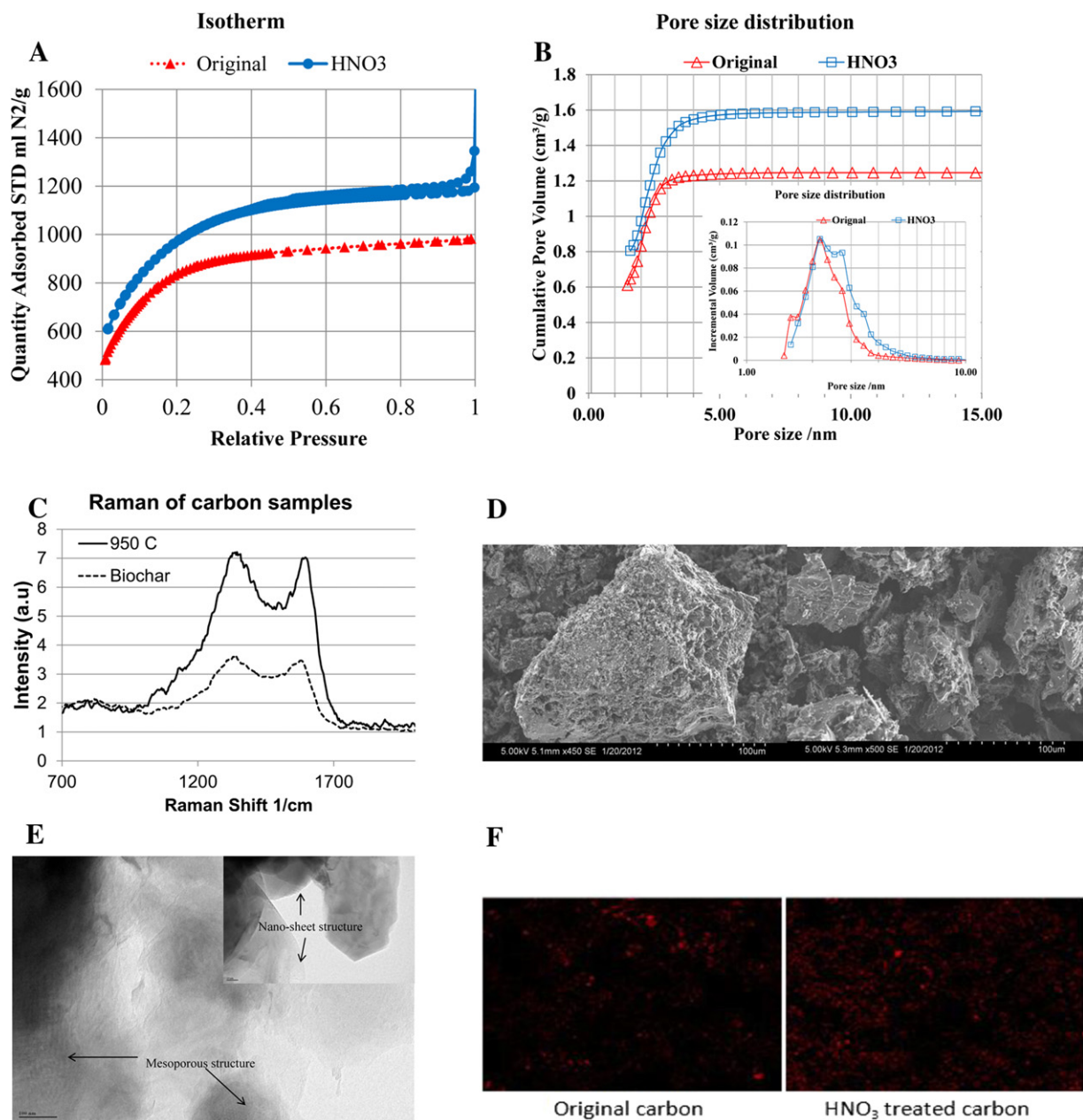

Fig. 1. (A) Impact for surface modification on N_2 isothermal adsorption on the hierarchical carbon (B) pore size distribution of the hierarchical carbon (C) Raman spectrum of the hierarchical carbon and biochar (D) SEM of biochar and the hierarchical carbon (E) TEM of the hierarchical carbon (F) Oxygen distribution from SEM-EDS.

Table 1
Surface area and pore structure parameters of the hierarchical carbon.

Sample	S_{BET}[a] (m^2 g^{-1})	V_t[b] (m^3 g^{-1})	V_{micro}[c] (m^3 g^{-1})	V_{meso}[d] (m^3 g^{-1})
Original Carbon	2959	1.65	0.83	0.42
HNO$_3$ Treated	3310	1.85	0.97	0.65

[a] BET (Brunauer–Emmett–Teller) surface area.
[b] Total pore volume, measured at $P/P_0 = 0.995$.
[c] Micropore volume, derived from NLDFT model.
[d] Mesopore volume, derived from NLDFT model.

well-developed mesoporous (2–5 nm) and microporous (<2 nm) structure, which was not only verified by its high surface area and identified mesoporous volume but also fast adsorption of methylene blue, which is generally applied as a model chemicals for quantifying mesoporous in porous carbon [19]. Furthermore, the surface area, pore volume and structure of the hierarchical carbon could be readily manipulated by changing the ratio of KOH versus biochar and activation temperature (Fig. S1). For KOH activation at 950 °C, BET surface area increased with increase in the dosage of KOH, till molar/mass ratio of base/biochar to 0.075, and then decreased slightly; while BET surface area just fluctuated around 2500 m^2 g^{-1} for activation using KOH at 1050 °C. It is similar to surface area that microporous volume also heavily depends on temperature and KOH loading, i.e. increased with dosage of KOH till molar/mass ratio of base/biochar to 0.075 at 950 °C. But at 1050 °C, microporous volume decreased heavily at high KOH loading (>0.05 mol g^{-1}). However total pore volume and mesopore volume increased with dosage of KOH and temperature.

In addition, after activation and washing, ash content in hierarchical carbon became extremely low (<0.01%). The Raman spectrum (Fig. 1C) of the hierarchical carbon displayed a characteristic intensity peak at 1580 cm^{-1} (G band) corresponding to a structure of individual graphene sheets and another intensity peak at 1360 cm^{-1} (D band) representative of disordered/turbostratic and imperfect structures found in the activated carbon [20]. The SEM images (Fig. 1D) of the microstructure in the hierarchical carbon clearly indicated that KOH activation process split the structures of DDGS biochar particles into small particles with layers structure. Furthermore, unlike traditional activated carbon, a structure of micro-layered graphene or graphite was observed in the TEM images (Fig. 1E). In addition, nanoporous structure was also observed in the TEM images (Fig. 1E). The layered graphene or graphite structure was rarely observed in general biomass derivate carbon materials [20]. However, carbon material with a layered graphene or oxidized graphitic sheets structure has been synthesized from biobased organic compounds such as sucrose, caramel or gelatin using mesopore silicate or silica as a template [14]. Furthermore, N-doped carbonaceous porous nanosheets have been synthesized from collagen cross-linked gel after pyrolysis in a nitrogen atmosphere [15].

Therefore, protein rich precursors and the high ash content in DDGS biochar are possible major factors in forming a nano-layered graphene or graphite structure. The mineral ash in biochar possibly performed as templates, i.e. a space constraint and substrate for carbon nanosheet growth in forming a layered structure [14]. However, how protein rich precursors form carbon nanosheets is still not clear and needs to be further investigated in the future.

After the HNO$_3$ hydrothermal treatment, the micropore volume increased from 0.83 to 0.97 cm^3 g^{-1}, which was also verified with increases in specific surface area. Compared to the original hierarchical carbon, the mesopore volume and total pore volume also increased about 0.20 cm^3 g^{-1} for the HNO$_3$ wet chemical oxidization.

It is noteworthy that after HNO$_3$ oxidation treatments, isothermal nitrogen adsorption–desorption curves shown a more

evident hysteresis loop between adsorption and desorption isotherms around relative pressures of 0.5–1.0 (Fig. 1A), which indicated a slit porous structure. The original carbon sample has significantly smaller mesopore volume than carbon samples treated with 4 M HNO$_3$, which showed two peak of mesoporous pores located in 2.2 and 2.8 nm, while the original carbon samples shows also clearly two peaks, one at 1.5 nm, and the other one at 2.2 nm (Fig. 1B). Thus, oxidization with HNO$_3$ increased both micropore and mesopore volume.

Furthermore after HNO$_3$ treatment, oxygen content in the activated carbon increased significantly, which has been verified by two different analytic methods, i.e. SEM-EDS (Table 2) and elements analysis (Table 3). Although, results of elements analysis (Table 3) showed higher oxygen content increase than SEM-EDS's result (Table 2), most oxygen groups were allocated on the surface of activated carbon after HNO$_3$ hydrothermal oxidization (Fig. 1F) because HNO$_3$ treatment is a surface oxidization methods [17]. In addition, hydrogen content in the activated carbon after HNO$_3$ treatment was almost doubled (Table 3), while nitrogen contents only increased slightly. According to the elements analysis results, the theoretic molecular structure of the original activated carbon was $C_{80}NHO_{2.46}$ and the HNO$_3$ treated carbon was $C_{80}NH_{2.15}O_7$. In other word, after HNO$_3$ treatment, 4.54 oxygen atoms were formed for every 80 carbon atoms, and the oxygen functional groups are more polar than the original carbon surface; which increased the wettability of activated carbon samples. As a result, the surface of activated carbon modified with HNO$_3$ was wet out immediately after contacting water drops, therefore a contact angle was impossible to measure, while droplets formed on electrodes fabricated from original activated carbon with contact angle 94–98° (Fig. S4).

Based on surface oxygen content and porous structure changes after HNO$_3$ hydrothermal treatment, the original activated carbon is further activated by HNO$_3$. Part of the carbon surface was developed into oxygen functional groups which are more polar than the original carbon surface [21].

3.2. Electrochemical capacitors from DDGS biochar derivate hierarchical carbons in aqueous electrolyte 6 mol L^{-1} KOH

With the prepared hierarchical carbon as the electrodes, the electrochemical behavior of the carbons, in a two-electrode symmetrical supercapacitor cell, was characterized with the CV galvanostatic charge–discharge cycles and EIS using the 6 M KOH as electrolytes. The information is concluded in Fig. 2.

According to CV curves of the supercapacitor at different scan rates at room temperature (Fig. 2A) DDGS biochar derivate hierarchical carbon exhibited symmetric capacitor performance in inorganic electrolyte, i.e. 6 mol L^{-1} KOH. For all hierarchical carbon samples, the shape of CV curves became more rectangular at lower scan rate, while the voltammetric currents increased with the increase of scan rate (Fig. 2A). In Fig. 2A, the HNO$_3$ treated carbon electrode showed more excellent square shape than the original carbon at all scan rates from 20 to 200 mV s^{-1}. According to this result, the HNO$_3$ treated carbon shows much better capacitor

Table 2
Elements composition from energy-dispersive X-ray spectroscopy (EDS).

Samples	Elements	Line	Intensity (c s^{-1})	Error 2-sig	Conc wt%
Original carbon	C	Kα	812.69	18.029	94.366
	O	Kα	15.66	2.503	5.634
HNO$_3$ treated carbon	C	Kα	608.88	15.606	90.399
	O	Kα	27.03	3.288	9.601

Table 3
Elements composition from elements analyzer.

Samples	C	N	H	S	O	Total
Original carbon	95.95	1.28	0.12	Non-detectable	3.93	100
HNO$_3$ treated carbon	89.43	1.34	0.24	Non-detectable	10.34	100

characteristic than the original carbon at all scan rates, i.e. from 20 to 200 mV s^{-1}. However Fig. 2A did not show the specific capacitance of electrodes, the current is just measuring results, which have not been divided by amount of active materials in electrodes.

In Fig. 2B the capacitance of the original hierarchical carbon decreased heavily with the faster current loads. For as-prepared

carbon samples, a specific capacitance of 260F g^{-1} was obtained at the current density of 100 mA g^{-1}, while the current density increased to 585 mA g^{-1}, the specific capacitance decreased around 30% to 200 F g^{-1}. In addition, according to galvanostatic charge–discharge curves (Fig. 2B), the original sample showed a small voltage drop, around 0.01 V, in the lower current density of 100 mA g^{-1}, while the current density increases to 585 mA g^{-1}; the supercapacitor showed an obvious voltage drop, about 0.1 V with the voltage between 0.8 V and 0.9 V. In order to obtain further electrochemical properties of the hierarchical carbon material, the electrochemical impedance spectroscopy is used to test the resistance of the cell type supercapacitor. The complex-plane impedances of the hierarchical carbon in inorganic electrolytes are shown
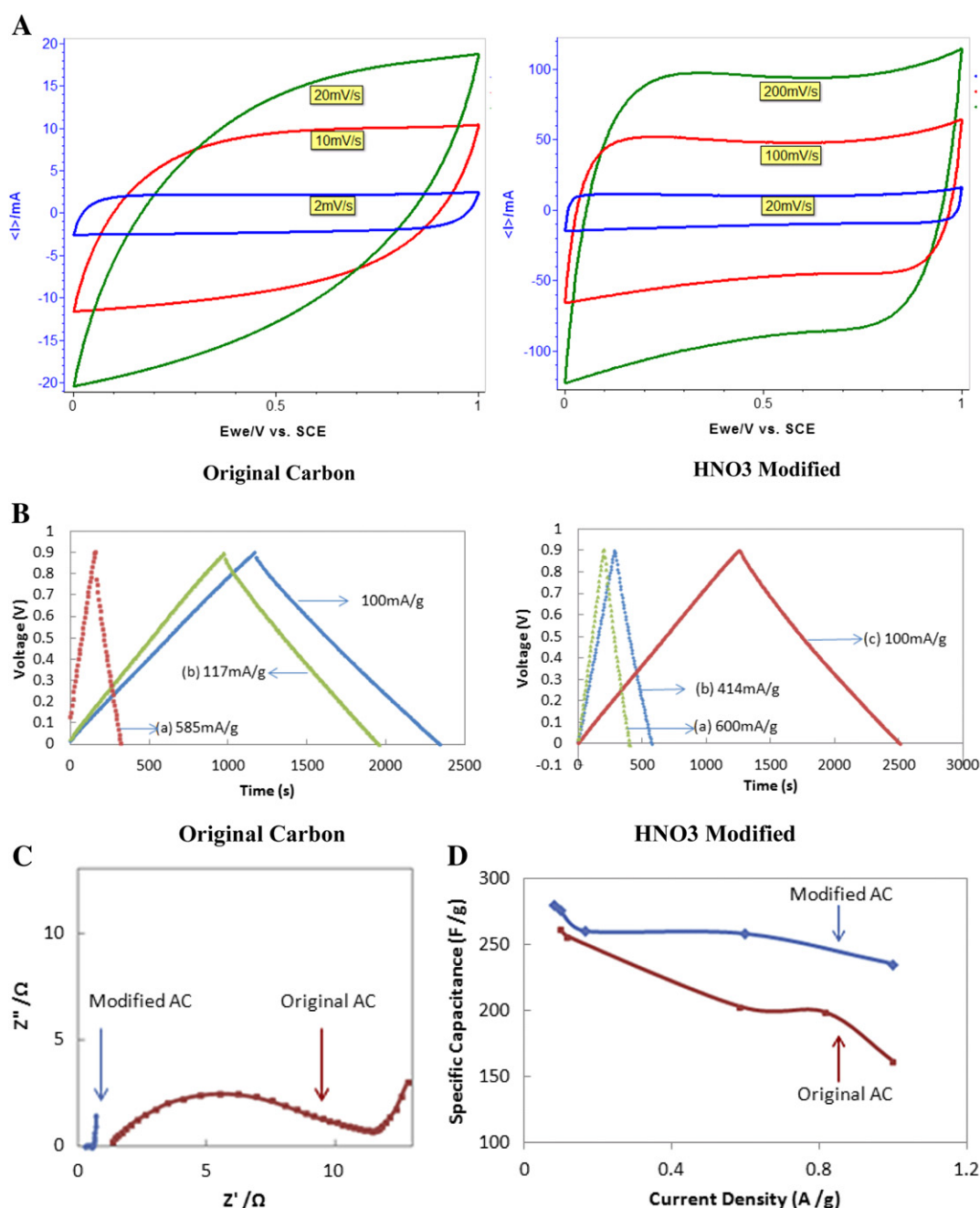

Fig. 2. (A) CV curve of the hierarchical carbon in 6 mol L^{-1} KOH. (B) Galvanostatic charge–discharge curve of the hierarchical carbon in 6 mol L^{-1} KOH. (C) EIS curve of the hierarchical carbon in 6 mol L^{-1} KOH. (D) Capacitance of the hierarchical carbon in 6 mol L^{-1} KOH at different current density.

in Fig. 2D, which showed the impedances corresponding to the frequency of 0.1—100,000 Hz. The impedances in high frequency region are mainly determined by the total resistance including resistance due to mass transferring and electrochemical reactions, electrolyte resistance and resistance of carbon matrix. Therefore, the semicircle in the high frequency indicates the equivalent serial resistance of the hierarchical carbon, which was around 13 Ω. This equivalent serial resistance of the hierarchical carbon was comparable to most bio-inspired amorphous carbon materials [3].

Although the original carbon sample did not exhibit adequate capacitor characteristic (i.e. lost rectangular shape) as the scan rate increases to 10 mV s^{-1}, which coincides with the galvanostatic charge—discharge test and electrochemical impedance spectroscopy results, after HNO$_3$ oxidation, the hierarchical carbon showed much better supercapacitor characteristic. After HNO$_3$ oxidation, the cyclic voltammograms of two-electrode supercapacitors showed more rectangular shape, even at scanning speed as high as 200 mV s^{-1}. In addition, for the HNO$_3$ modification samples, the supercapacitors showed much more rectangular shape galvanostatic charge—discharge curve at the current density from 100 mA g^{-1} to 600 mA g^{-1} without any visible voltage drop, which was much better than as-prepared hierarchical carbon. After oxidization, the specific capacitance of the supercapacitor only decreased about 5% with the current density increase from 100 mA g^{-1} to 600 mA g^{-1}. Although the hierarchical carbon, treated with 4 M HNO$_3$, only showed slightly higher specific capacitance of 275F g^{-1} at the current density of 100 mA g^{-1} than the original carbon, HNO$_3$ oxidation significantly improved energy storage capacitance (i.e. 260 F g^{-1}) at higher power loading (i.e. charging and discharging at current density 600 mA g^{-1}) (Fig. 2D). This high stability of specific capacitance was much more acceptable than the original hierarchical carbon material, especially for future potential commercial application.

Results of water contact angle of original and HNO$_3$ treated carbon indicated a significant change of wettability of carbon materials after HNO$_3$ hydrothermal modification. The surface of activated carbon modified with HNO$_3$ was wet out immediately after contacting water drops, therefore a contact angle was impossible to measure, while droplets formed on electrodes fabricated from original activated carbon. This drastic wettability change in surface were mainly caused by surface oxygen functional groups generated in HNO$_3$ hydrothermal oxidization of the carbon because all electrodes were fabricated from carbon materials with same particles (200—300 mesh) and similar porous structure using the same protocol.

Furthermore, the electrochemical impedance spectroscopy showed that equivalent serial resistance of the oxidized hierarchical carbon decreased significantly to only around 0.5 Ω for HNO$_3$ oxidation respectively. The internal resistance of HNO$_3$ oxidized hierarchical carbon was even comparable to graphene i.e. 0.4 Ω under same analysis condition (Fig. S2B). This significant internal resistance decrease was possibly caused by wettability changes, which has been indicated by water contact angle tests' results. After HNO$_3$ hydrothermal modification, water drops disappeared immediately after contacting electrodes surface, while water contact angle 94—98° was measured on electrodes of original carbon. Therefore after HNO$_3$ treatment, surface hydrophobicity of DDGS biochar based activated carbon was changed from partial hydrophobic to extreme hydrophilic because of significant amount of surface oxygen functional groups (Tables 2 and 3 and Fig. 1F). As a result, inorganic electrolyte only partially wetted the surface of original activated carbon, while surface of HNO$_3$ treated carbon was wetted completely. In addition, supercapacitors, composed of HNO$_3$ treated carbon and commercial graphene, showed the impedance spectra approached to a vertical line at low frequencies (Fig. 2C and Fig. S2B), which indicates ideal capacitive performance of the HNO$_3$

treated carbon and commercial graphene [22]. However, different from commercial graphene, the DDGS biochar derivate hierarchical carbon without HNO$_3$ oxidation treatment showed inclined curve at low frequency, which indicated that there was some capacitance from faradaic capacitive behavior. This result might be caused by interaction between electrolytes and surface functional groups of the original hierarchical carbon, and the increase of electrolyte ions diffusion resistance due to the electrolytes entered into micropores, while the wettability of the aqueous electrolyte and the resistance of the ion transportation were greatly improved after HNO$_3$ oxidation treatment due to increases of surface oxygen functional groups (Fig. 1F and Tables 2 and 3). On the other hand, graphene is layers structure, which supplies fast mass transfer channels for ions.

In general, the conductivity of carbon materials is mainly determined by graphitization intensity, porous structure and surface heterogenous elements, such as oxygen and nitrogen groups. In most cases, additional functional groups decrease the material's electron conductivity because the surface groups inhibit electron transport among the intrinsic crystal structures of the electrode. However, functional groups greatly improve the ions mobility in porous structure by enhancing their accessibility to active surface areas and reduce the ohmic drop of the electrolyte during charge/discharge. Impact of surface oxygen functional groups was more evident in this study, the internal resistance of hierarchical carbon decreased heavily with treatments using HNO$_3$ possibly because of faster forming of electrical doublelayers, which might be partially caused by increase in mesopore volume. Besides increase of pore size and volume, after HNO$_3$ hydrothermal treatment, additional surface oxygen groups (Fig. 1F, Tables 2 and 3) improved the wettability of carbon surface by increasing hydrophilicity [18], which was verified by significant decrease of water contact angles (i.e. decreased from 94 to 98° to non-measurable) after HNO$_3$ hydrothermal treatment. Therefore, surface oxidization enhanced the formation of electric doublelayer in aqueous liquid phase. On the other hand, the HNO$_3$ oxidation might also bring nitrogen groups into the matrix or the internal pore surface of carbon, which have been proved to increase the capacitance of electrodes by inducing Faradaic reactions [23]. Furthermore, HNO$_3$ treatment not only increased the specific capacitance, but also changed the cyclability of supercapacitors. The HNO$_3$ hydrothermally modified activated carbon shown significant capacitance decrease in the initial cycles (Fig. S3), while original activated carbon shown a capacity increase in first ten cycles, which indicated a surface wetting procedure. This hypothesis was also verified by contact angle analysis, in which original carbon shown contact angle of water at around 94—98° while water wetting HNO$_3$ treated carbon immediately without measurable contact angle. As a result, surface oxidization significantly improved energy storage performance, at high power, of carbon electrodes in supercapacitors. This capacitance improvement at high power was mainly due to the decrease of internal resistance and the increase of mesoporous volume.

It is noteworthy that the specific capacitance of the hierarchical carbons was even higher than commercial graphene (Grade C from XGScience Inc). The commercial graphene only showed capacitance about 120 F g^{-1} at a current density 200 mA g^{-1} in 6 mol L^{-1} KOH (Fig. S2A). The specific capacitance of the hierarchical carbon was also higher than chemical activated graphene, which only achieved 154 F g^{-1} at 500 mV s^{-1} in 6 mol L^{-1} KOH [24].

The HNO$_3$ oxidized hierarchical carbon' specific capacitance, i.e. 260 F g^{-1} at current density 0.6 A g^{-1} was even better than multiple bio-inspired carbon materials, which were special designed for application in supercapacitor [17]. More reported specific capacitance of different carbon materials in inorganic electrolytes were cited and compared to the hierarchical carbon prepared in this work (Table 4). According to data shown in Table 4, the DDGS

Table 4
Specific capacitances parameters of different carbon materials.

Carbon resource	Carbon type (activation methods)	Capacitance F g^{-1} (electrolytes)	Current density A g^{-1}	Literature
DDGS	Hierarchical carbon (KOH) and HNO$_3$ oxidation	260(6 M KOH) 230*	0.6 1.0*	This work
TiC	Carbide derivate carbon (Cl$_2$)	102 (1 M H$_2$SO$_4$)	1.7	[4]
Pig bone	Activated carbon (KOH)	185 (7 M KOH)	0.05	[25]
Graphene	Activated graphene (MnO2)	200 (6 M KOH)	100 mV s^{-1}	[24]
Banana peel, furfural and 2-aminophenol	Activated carbon (ZnNO$_3$)	206 (6 M KOH)	1 A g^{-1}	[26]
Sucrose	OMC	203 (6 M KOH)	1 A g^{-1}	[27]
Graphene-p-phenylene diamine	Activated carbon-Graphene (KOH)	150 (6 M KOH)	1 A g^{-1}	[28]
Graphene	Graphene	135 (5.5 M KOH)	1.3 A g^{-1}	[29]

M: mol L^{-1}.

biochar derivate hierarchical carbon after HNO$_3$ oxidation showed comparable capacitance to most bio-inspired carbon, metal carbides derivate carbon (CDC) and organized mesoporous carbon (OMC), even some graphene materials at similar or comparable current density.

DDGS biochar derivate hierarchical carbons also showed stable recycle capacitance, more than 99% of its capacitance was retained after 2000 constant current charge/discharge cycles at a current density of 600 mA g^{-1} in 6 mol L^{-1} KOH electrolyte (Fig. 2C). Furthermore, in electrodes composed of porous carbon, the total capacitance included capacitance of different pore structures and sizes. The specific capacitance of porous carbon materials in 6 KOH generally ranged from 0.05 to 0.2 F m^{-2} in recent review report of supercapacitors [3]. For the DDGS biochar derivate hierarchical carbon after HNO$_3$ oxidation, this value was around 0.08 F m^{-2} coincident with the reported range. Although this value is lower than most CDC or OMC, i.e. 0.10–0.2 F m^{-2}. This is the first time to develop carbon materials for supercapacitor from thermochemical pyrolysis residues i.e. biochar.

4. Conclusions

Sustainable production of hierarchical carbon from DDGS high ash biochar using KOH as the activation agent was developed and the results reported. Hierarchical carbon samples containing a layered nanostructure similar to that of activated graphene were prepared at 950 °C with KOH dosages of 0.075 mol g^{-1}. A supercapacitor has also been developed at SDSU using 6 mol L^{-1} KOH as the electrolyte with electrodes composed of the hierarchical carbon prepared with KOH (0.075 mol g^{-1} biochar) at 950 °C. The hierarchical carbon showed stable high reversible capacitance (260 F g^{-1} at a constant current of 0.1 A g) for more than 2000 cycles. In addition surface oxidation with HNO$_3$ treatment significantly improve capacitance performance of the hierarchical carbon materials in supercapacitor at high current density i.e. 600 mA g^{-1}. Based on the test results reported within this paper, DDGS biochar derivate hierarchical carbon has the potential to be a lower cost substitute for advanced carbon materials currently derived from metal carbides, graphene or activated graphene. The synthesis process is well industrialized and directly without artificial template and complicates procedures, which are generally used in preparation of mesoporous carbon. Biochar feedstock is more economic than graphene and metal carbide for activated graphene and CDC respectively. Furthermore, the performance as electrode materials in supercapacitor was tested with well-established commercial current collectors, binders, conduct additives, electrolytes and separators. Therefore the high capacitance performance is readily to be achieved in industrial environment in a short period.

The other potential benefits of this work is to enhance economic viability of thermochemical biofuel platform with a value added co-product, i.e. advanced hierarchical carbon materials for fast growing market in electrical energy storage.

Acknowledgments

Appendix A. Supplementary data

Supplementary data related to this article can be found at http://dx.doi.org/10.1016/j.jpowsour.2013.02.088.

References

[1] E. Frackowiak, Phys. Chem. Chem. Phys. 9 (2007) 1774–1785.
[2] Y.W. Zhu, S. Murali, M.D. Stoller, K.J. Ganesh, W.W. Cai, R.S. Ruoff, Science 332 (2011) 1537–1539.
[3] A. Ghosh, Y.H. Lee, ChemSusChem 5 (2012) 480–499.
[4] V. Presser, L.F. Zhang, J.J. Niu, J. McDonough, C. Perez, H. Fong, Y. Gogotsi, Adv. Energy Mater. 1 (2011) 423–430.
[5] X. Li, W. Xing, S.P. Zhuo, J. Zhou, F. Li, S.Z. Qiao, G.Q. Lu, Bioresour. Technol. 102 (2011) 1118–1123.
[6] K. Kuratani, K. Okuno, T. Iwaki, M. Kato, N. Takeichi, T. Miyuki, M. Majima, T. Sakai, J. Power Sources 196 (2011) 10788–10790.
[7] M.S. Balathanigaimani, W.G. Shim, M.J. Lee, C. Kim, J.W. Lee, H. Moon, Electrochem. Commun. 10 (2008) 868–871.
[8] Q.Q. Li, F. Liu, L. Zhang, B.J. Nelson, S.H. Zhang, C. Ma, X.Y. Tao, J.P. Cheng, X.B. Zhang, J. Power Sources 207 (2012) 199–204.
[9] E. Ito, S. Mozia, M. Okuda, T. Nakano, M. Toyoda, M. Inagaki, New Carbon Mater. 22 (2007) 321–326.
[10] C.E. Brewer, K. Schmidt-Rohr, J.A. Satrio, R.C. Brown, Environ. Prog. Sustain. Energy 28 (2008) 386–396.
[11] R. Azargohar, A.K. Dalai, Microporous Mesoporous Mater. 110 (2008) 413–421.
[12] I.M. Lima, A.A. Boateng, K.J. Klasson, J. Chem. Technol. Biotechnol. 85 (2010) 1515–1521.
[13] G.D. Ruan, Z.Z. Sun, Z.W. Peng, J.M. Tour, Acs Nano 5 (2011) 7601–7607.
[14] R.H. Eduardo, D. Margarita, M.F. Francisco, Z. Ezzouhra, Adv. Mater. 23 (2011) 5250–5255.
[15] Y.H. Lee, Y.F. Lee, K.S. Chang, C.C. Hu, Electrochem. Commun. 13 (2011) 50–53.
[16] H.W. Lei, S.J. Ren, L. Wang, Bioresour. Technol. 102 (2011) 6208–6213.
[17] M. Inagaki, H. Konno, O. Tanaike, J. Power Sources 195 (2010) 7880–7903.
[18] L.P. Zheng, Y. Wang, X. Wang, X.Y. Wang, H.F. An, L.H. Yi, J. Mater. Sci. 45 (2010) 6030–6037.
[19] F. Raposo, M.A. Rubia, R. Borja, J. Hazard. Mater. 165 (2009) 291–299.
[20] P. Oskar, C. Zollfrank, G.A. Zickler, Carbon 43 (2005) 53–66.
[21] M.A. Wan, D. Wan, A.H. Houshamnd, J. Nat. Gas Chem. 19 (2010) 267–279.
[22] B.E. Conway, Electrochemical Supercapacitors: Scientific Fundamentals and Technological Applications, Kluwer–Plenum Press, New York, 1999.
[23] S. Candelaria, B. Garcia, D. Liu, G. Cao, J. Mater. Chem. 22 (2012) 9884–9889.

[24] Z.J. Fan, Q.K. Zhao, T.Y. Li, J. Yan, Y.M. Ren, J. Feng, T. Wei, Carbon 50 (2012) 1699–1712.

[25] W.T. Huang, H. Zhang, Y.Q. Huang, W.K. Wang, S.C. Wei, Carbon 49 (2011) 838–843.

[26] Y.K. Lv, L.H. Gan, M.X. Liu, W. Xiong, Z.J. Xu, D.Z. Zhu, D.S. Wright, J. Power Sources 209 (2012) 152–157.

[27] H.L. Lu, W.J. Dai, M.B. Zheng, N.W. Li, G.B. Ji, J.M. Cao, J. Power Sources 209 (2012) 243–250.

[28] Y. Chen, X. Zhang, H.T. Zhang, X.Z. Sun, D.C. Zhang, Y.W. Ma, RSC Adv. 2 (2012) 7747–7753.

[29] M.D. Stoller, S.J. Park, Y.W. Zhu, J.H. An, R.S. Ruoff, Nano Lett. 8 (10) (2008) 3498–3502.